Local extinction-reignition in turbulent nonpremixed combustion

By Paiboon Sripakagorn†, George Kosály† AND Heinz Pitsch

1. Introduction

Recent reports demonstrate progress in the modeling of burning diffusion flames in the absence of extinction (International Workshop on Measurement and Computation of Turbulent Nonpremixed Flame(2000)). However, the prediction of flames whose burning is frequently interrupted by local extinction-reignition events still presents a major modeling problem (Peters (2000)).

A recent report by Xu & Pope (1999) shows promising results in modeling of a combusting flame with considerable extinction. Xu & Pope use a PDF modeling approach that is known to be expensive computationally. There is incentive, therefore, to study possible generalizations of the mixture fraction based approaches (flamelet, CMC) that would account for local extinction-reignition events.

The present paper reports on direct numerical simulation (DNS) of initially nonpremixed fields of fuel and oxidizer developing in a turbulent field. Initially, the scalar dissipation rate is increasing due to straining leading to localized extinction events. At later times molecular diffusion starts to decrease the scalar dissipation rate, resulting in gradual reignition.

Flame element tracking is utilized to show the fields as they would appear in local coordinate systems fixed to different points on the $Z_{\rm st}$ surface. The resulting data are used (a) to study the mechanism of extinction and especially reignition, (b) to elucidate the applicability of the flamelet model to describe these processes, and (c) to examine a possible extension of the model to account for lateral heat diffusion along the $Z_{\rm st}$ surface.

2. DNS of local extinction-reignition and flame element tracking

2.1. *Direct numerical simulation*

2.1.1. *Velocity field*

The simulated velocity field is incompressible decaying isotropic turbulence comparable to the turbulence downstream of a laboratory grid. The main parameters of the initial velocity and scalar fields are shown in Table 1.

As pointed out by Eswaran & Pope (1988), to resolve the small scales, the resolution condition $\eta_{\rm k} k_{\rm max} > 1$ must be met (see also Mell *et al.* (1994)). Here the parameter $k_{\rm max}$ is the wave number cutoff while $\eta_{\rm k}$ is the Kolmogorov scale of the velocity. To resolve quantities involving derivatives, $\eta_{\rm k} k_{\rm max} > 1.5$ is to be satisfied (Yeung & Pope (1989)).

The computational domain is a cube with the size of 2π using periodic boundary conditions at all sides. The integral length scale, l, must be kept adequately small so that the boundary conditions do not influence the results. The condition is $l\Delta k \leq O(1)$ where the smallest nonzero wavenumber is $\Delta k = 2\pi/L$ for the computational box of size L.

† University of Washington, Seattle, WA 98195-2600

$k_{\max}\eta_{\rm k}$	l (cm)	u/l (1/s)	$l/\eta_{\rm k}$	ν (cm/s^2)	Re_λ	N^3	l_Z/l	Sc
1.94	0.879	1.04	27.2	0.01	33	128^3	0.968	0.7

TABLE 1. Initial conditions used in the DNS of the flow field and the mixture fraction field.

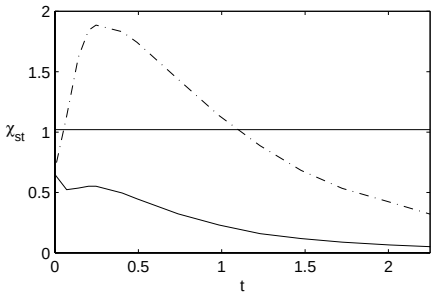

FIGURE 1. The time evolution of $\chi_{\rm st}$. Here $\chi_{\rm st}$ is the scalar dissipation rate at $Z = Z_{\rm st} = 0.5$. ——— : $\langle\chi_{\rm st}\rangle$, - - - - : 99% envelope of the fluctuations of $\chi_{\rm st}$. The horizontal line is drawn at $\chi_{\rm st} = \chi_{\rm q} = 1.02$. This is the largest possible value of $\chi_{\rm st}$ where the steady flamelet equation has a burning solution. The numerical value refers to the chemistry parameters shown in Table 2.

2.1.2. *Scalar fields*

The initial mixture fraction is arranged in blobs of Z=0 and Z=1. The fuel blobs fill half of the computational domain; the average value of the mixture fraction ($\langle Z\rangle$) is close to 0.5. In the quasi-steady flamelet model (Peters (1983)), the mass fractions depend on space and time through the local, instantaneous values of Z and χ ($\chi = 2D|\nabla Z|^2$, the scalar dissipation rate). The fuel and oxidizer fields are initialized via the quasi-steady flamelet model.

The scalars are initialized when the characteristic length scales of the velocity field start to increase with time. This condition corresponds to a fully developed turbulent flow undergoing full spectrum decay. Once the scalars have been injected, turbulent strain creates large scalar gradients, and the magnitude of the scalar dissipation rate χ increases significantly. Due to the many different turbulent scales involved, the scalar dissipation rates induced by the straining fluctuate strongly (Fig. 1). It is only later that molecular mixing overcomes the influence of turbulent straining and leads to the decrease of the scalar gradients. This paper examines the extinction-reignition phenomena caused by the increase and subsequent decrease of the scalar dissipation rate shown in Fig. 1.

2.1.3. *Simulations*

The simulated velocity field evolves according to the incompressible Navier-Stokes equations,

$$\nabla \cdot \bar{u} = 0 \tag{2.1}$$

$$\frac{\partial \bar{u}}{\partial t} = \bar{u} \times \bar{w} - \nabla\{p - \frac{|\bar{u}|^2}{2}\} + \nu\nabla^2\bar{u}, \tag{2.2}$$

where $\bar{w}$ denotes the vorticity vector and p is the hydrodynamic pressure. The kinematic viscosity, ν, is independent of the temperature.

The mixture fraction and species mass fractions satisfy the conservation equation

$$\frac{\partial Y_i}{\partial t} = -u \cdot \nabla Y_i + D\nabla^2 Y_i - w_i. \tag{2.3}$$

Here D is the coefficient of molecular diffusion, $D = \nu/Sc$. In the Z-equation the reaction rate is zero.

The set of governing equations was solved using a pseudospectral code developed by Nilsen (1998). The spatial derivative fields were evaluated in Fourier space while nonlinear terms such as $\bar{u} \times \bar{w}$ or $\bar{u} \cdot \nabla Y_i$ were computed in physical space. The time advancement was done by a second-order Adams-Bashforth scheme.

2.2. *Flame element tracking*

2.2.1. *Flame elements*

Unless the chemistry is slower than molecular mixing, the reaction zone is close to the instantaneous stoichiometric surface, defined as $Z(\bar{x}, t) = Z_{\rm st}$. The phrase "flame element" in this paper means a point on the instantaneous $Z_{\rm st}$ surface.

The $Z_{\rm st}$ surface moves relative to the laboratory reference frame. Gibson (1968) points out that the velocity of a point fixed on an isoscalar surface relative to the laboratory reference frame can be given as

$$\bar{u}_Z = \bar{u} - \frac{D\nabla^2 Z}{|\nabla Z|}\bar{i}_Z = \bar{u} - D\nabla^2 Z \frac{\nabla Z}{|\nabla Z|^2} \tag{2.4}$$

Here $\bar{u}$ is the fluid velocity and $\bar{i}_Z$ is the unit vector in the direction of local mixture fraction gradient. Since the $Z_{\rm st}$ surface is an isoscalar surface, the instantaneous velocity of a flame element can be calculated from Eq. (2.4).

Note that flame elements are not fluid particles. Fluid particles are convected by the velocity field. The second term on the RHS of Eq. (2.4) accounts for propagation due to molecular diffusion (Gibson (1968)). While several authors have used simulated and laboratory data to track fluid particles (Shlien & Corrsin (1974), Sato & Yamamoto (1987), Yeung & Pope (1989)), the technique of flame element tracking has been introduced by Mell *et al.* (1994). This paper uses flame element tracking to show the fields as they would appear in the frame of reference of an observer fixed to a point on the instantaneous $Z_{\rm st}$ surface.

2.2.2. *Methodology*

A number of selected points located on the $Z_{\rm st}$ surface were tagged in the initial scalar field. Since the velocity and mixture fraction fields are known from the DNS, the velocity of the points on the isoscalar surface is available from Eq. (2.4). Since the DNS fields are available on a 3-dimensional grid, an accurate interpolation scheme is needed to determine the velocity data between grid points. The updated positions of the flame elements can be obtained by integrating the equations of motion.

The accuracy of the interpolation scheme is crucial to the particle tracking routine. Yeung & Pope (1988) have compared results obtained from a 3^{rd}-order, 13 points Taylor series (TS13) scheme and another scheme working with 4^{th} order cubic splines. The approach via cubic splines was found to be our method of choice. The goal of this method is to get a formula that is smooth in the first derivative and continuous in the second derivative, both within an interval and at its boundaries. The resulting twice continuously

$Z_{\rm st}$	r	α	β	K
0.5	1.0	0.87	4.0	100

TABLE 2. Numerical values used for the thermochemistry parameters defined in Section 3.1.

differentiable approximation of the interpolated variables leads to a low level of numerical noise in the time series obtained. Regarding the integration scheme, Yeung & Pope (1988) have shown that an explicit 2^{nd}-order Runge-Kutta scheme works well. This method has been also applied by Squires & Eaton (1991) and Elghobashi & Truesdell (1993).

In this study the 4^{th}-order accurate cubic spline interpolation has been implemented for the interpolation scheme. For the time stepping, the 2^{nd}-order Runge-Kutta scheme has been employed. The details of the interpolation method can be found in Yeung & Pope (1988). Note, however, that due to the possibility of large flame stretching and the highly three-dimensional structure of the isoscalar surface, the tagging location might start to wander away from the isoscalar surface by a small amount every timestep. A surface-searching module has been added to the tracking code to return the tagged flame element onto the the $Z_{\rm st}$ surface once every few timesteps.

3. Turbulent combustion model

3.1. *Chemistry scheme*

A single-step reversible reaction has been considered with an Arrhenius-type pre-exponential factor.

$$F + rO \quad \leftrightharpoons \quad (r+1)P \tag{3.1}$$

Considering identical equilibrium constants for the forward and backward reactions, the production rate of the product can be written (Lee & Pope (1995))

$$w_p = (r+1)A_o \exp\left(\frac{-\beta}{\alpha}\right) \exp\left[\frac{-\beta(1-Y_p)}{1-\alpha(1-Y_p)}\right] \left(Y_f Y_o - \frac{1}{K} Y_p^2\right). \tag{3.2}$$

Here r is the mass of oxidizer disappearing with unit mass of fluid; Y_f, Y_o, and Y_p stand for the mass fractions of fuel, oxidizer, and product in order.

Throughout the paper the fresh values of the fuel and oxidant mass fractions are considered unity; therefore, the stoichiometric value of the mixture fraction is given as $Z_{\rm st} = 1/(1+r)$. The present choice is $r = 1$, this means, $Z_{\rm st} = 0.5$. The reaction kinetics is characterized by the following dimensionless quantities:

$$\text{Zel'dovich number,} \quad \beta = \frac{T_a}{T_b}\frac{T_b - T_u}{T_b} \tag{3.3}$$

$$\text{Heat-release parameter,} \quad \alpha = \frac{T_b - T_u}{T_b} \tag{3.4}$$

$$\text{Reduced temperature,} \quad \Theta = \frac{T - T_u}{T_b - T_u} \tag{3.5}$$

where T_a is the activation temperature, T_b is the adiabatic flame temperature, and T_u

FIGURE 2. The local coordinate system used in flamelet modeling. Point O is fixed on the stoichiometric surface.

is the (equal) temperature of the fuel and oxidizer streams. For this case, Θ is equal to Y_p. Table 2 shows the values of the thermochemistry parameters used in the simulations. The parameters were selected to lead to local extinction-reignition in a strongly burning flame (Overholt & Pope (1999)).

3.2. *Flamelet modeling*

Figure 2 shows a local coordinate system fixed to a point (point O) on the $Z_{\rm st}$ surface. Axes x_1 and x_2 are locally (close to point O) tangential to the $Z_{\rm st}$ surface, whereas the mixture fraction coordinate is locally perpendicular to the surface. Note that this coordinate system cannot be used to describe local burning unless the reaction zone is sufficiently thin in space, and, therefore, the mixture fraction changes monotonically along the direction that is locally perpendicular to the $Z_{\rm st}$ surface.

From the point of view of the observer located at point O (traveling with it) the mass fractions are dependent on the variables t, Z, x_1, and x_2 . Straightforward calculations show (Peters (1983), (1984)) that in the local coordinate system the mass fraction $Y_i = Y_i(t, Z, x_1, x_2)$ satisfies the following equation:

$$\begin{aligned}&\frac{\partial Y_i}{\partial t} - \frac{\chi}{2}\frac{\partial^2 Y_i}{\partial Z^2}\\ &= -\left(v_2\frac{\partial Y_i}{\partial Z_2} + v_3\frac{\partial Y_i}{\partial Z_3}\right) + 2D\left(\frac{\partial Z}{\partial x_2}\frac{\partial^2 Y_i}{\partial Z\partial Z_2} + \frac{\partial Z}{\partial x_3}\frac{\partial^2 Y_i}{\partial Z\partial Z_3}\right) + D\left(\frac{\partial^2 Y_i}{\partial Z_2^2} + \frac{\partial^2 Y_i}{\partial Z_3^2}\right) + w_i\end{aligned} \tag{3.6}$$

where the scalar dissipation rate, χ is defined by $\chi = 2D(\nabla Z^2)$.

In the time dependent flamelet model (TFL) (Peters (1983), (1984)) the first three terms on the RHS are neglected compared to the term describing mixing across the $Z_{\rm st}$ surface (second term on the LHS). The model equation reads then (Peters (1983), (1984))

$$\frac{\partial Y_i}{\partial t} - \frac{\chi}{2}\frac{\partial^2 Y_i}{\partial Z^2} = w_i \tag{3.7}$$

Neglecting the time derivative in Eq. (3.7) the (quasi) steady flamelet model (SFL) follows (Peters (1983), (1984))

$$-\frac{\chi}{2}\frac{\partial^2 Y_i}{\partial Z^2} = w_i. \tag{3.8}$$

The three terms neglected on the RHS of Eq. (3.6) represent lateral convection, curvature, and lateral diffusion at O. The neglection of these terms in Eq. (3.7) and the neglection of the time derivative in Eq. (3.8) are related to the thinness of the reaction zone in mixture fraction space. Thin reaction zones are due to high values of the local Damköhler number.

Presently we assume that the scalar dissipation rate (χ) appearing in Eqs. (3.6-3.8)

can be modeled using

$$\chi(Z) = \chi_{\rm st} F(Z), \tag{3.9}$$

where the form function, $F(Z) = \exp[-2(\mathrm{erf}^{-1}(2Z-1)^2)]$ has been used. This modeling assumes that close to point O the mixing is "counterflow-like". The simulations were designed such that this approximation shall be approximately valid.

3.3. *Interacting flamelet model*

According to Eqs. (3.7-3.8) the temperature at a point on the $Z_{\rm st}$ surface evolves under the influence of its own scalar dissipation rate; neighboring points have no influence on its temperature. Even the closest neighbors extinguish and reignite as isolated counterflows (auto-ignition). This behavior is due to the neglection of the first three terms on the RHS of Eq. (3.6) that represent lateral coupling (interaction) between neighboring points (cf. Fig. 2). We presently refer to Eq. (3.6) as the model equation of the interacting flamelet approach.

One of the goals of the present paper is to examine the role of the lateral interactions in extinction-reignition phenomena. To simplify the task let us write Eq. (3.6) at point O (Z=0.5, $Z_2 = Z_3 = 0$ in Fig. 2). The coordinate system shown in Fig. 2 propagates with the velocity of O, and at O the $Z_2 - Z_3$ plane is tangential to the $Z_{\rm st}$ surface. This means that at point O the first two interaction terms in Eq. (3.6) are zero; only the lateral diffusion term is left in the equation. We denote this lateral diffusion term by i_3.

$$\frac{\partial Y_i}{\partial t} - \frac{\chi_{\rm st}}{2}\left(\frac{\partial^2 Y_i}{\partial Z^2}\right)_{Z=0.5, Z_2=Z_3=0} - i_3 = w_i \tag{3.10}$$

$$i_3 \equiv D\left(\frac{\partial^2 Y_i}{\partial Z_2^2} + \frac{\partial^2 Y_i}{\partial Z_3^2}\right)_{Z=0.5, Z_2=Z_3=0}. \tag{3.11}$$

3.4. *Implementation*

The tracking procedure provides us with the entire temperature and scalar dissipation rate history of the flame elements we are tracking. Hence, it is possible to implement the time-dependent flamelet model (TFL), i.e. Eq. (3.7), for each tracked flame element. Since the DNS is initialized with the steady flamelet model, the TFL computations are initialized the same way.

The flamelet equation is solved by the flux-splitting technique. The diffusion term is advanced by the implicit Crank-Nicolson method while the source term is handled using the 2^{nd}-order Adam-Bashford approach. For simplicity a uniform grid of sufficient gridsize is used. The steady flamelet solution (SFL) is identified as the burning branch of the S-curve and is evaluated from Eq. (3.8) using the same set of codes. For the present chemistry parameters (Table 2), SFL gives $\chi_{\rm st} = \chi_{\rm q} = 1.02$ as the extinction limit. Above this limit Eq. (3.8) has no burning solution.

We remind the reader that Eq. (3.10) is valid only at point O indicated in Fig. 2. We will use information from the vicinity of this point to investigate the possibility of describing extinction-reignition via TFL and to look for possible correlation between the reignition process and the time evolution of the i_3 term. To obtain the value of the i_3 term, instead of evaluating the two 2^{nd}-derivative terms separately, the following relationship is used.

$$\frac{\partial^2 Y_i}{\partial Z_2^2} + \frac{\partial^2 Y_i}{\partial Z_3^2} = \nabla^2 Y_i - \frac{\partial^2 Y_i}{\partial x_1^2} \tag{3.12}$$

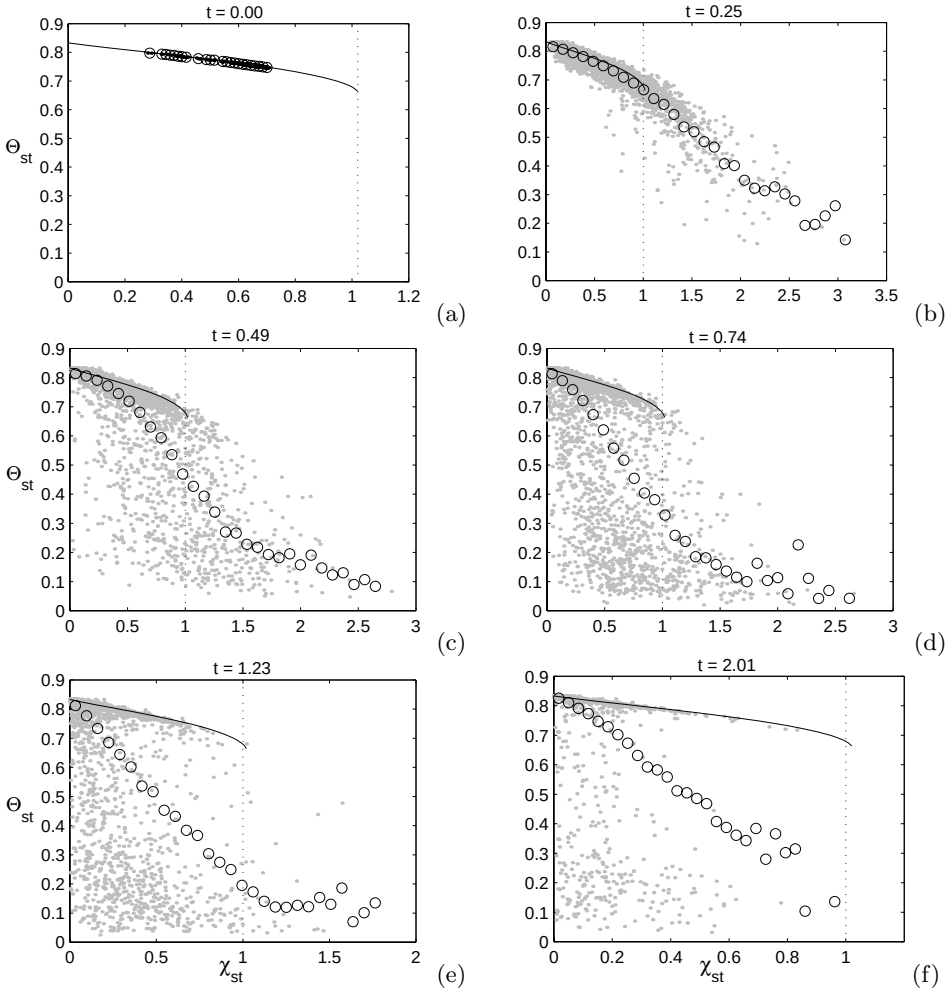

FIGURE 3. Extinction-reignition behavior on the $Z_{\rm st}$ surface. ——— : burning solution of the steady-flamelet equation. ∘ : average temperature for chosen values of the scalar dissipation rate ($\langle\Theta|Z_{\rm st},\chi_{\rm st}\rangle$). The grey dots represent the temperature of 5000 randomly selected flame elements. The vertical dotted line is at $\chi_{\rm st}=\chi_{\rm q}$.

The Laplacian of Y_i is easy and accurate to use to evaluate from the laboratory coordinate; the 2^{nd}-derivative in the Z-direction can be obtained from Eulerian data in the DNS. The 4^{th}-order central-difference formula was used to return the 2^{nd}-derivative on the right-hand side of Eq. 3.12.

4. Results and discussion

4.1. *Extinction and reignition: DNS*

Figure 3 exhibits the extinction and reignition behavior of the DNS field. The figure refers to $Z=Z_{\rm st}$. The broken line indicates the burning branch of the steady-flamelet solution, the circles show the conditional average of the temperature for fixed value of $Z=Z_{\rm st}$ and $\chi=\chi_{\rm st}$ as computed from the data ($\langle\Theta|Z_{\rm st},\chi_{\rm st}\rangle$). The vertical dotted line is at $\chi_{\rm st}=\chi_{\rm q}$. The reacting scalar field was initialized on the broken line (Fig. 3a). Very

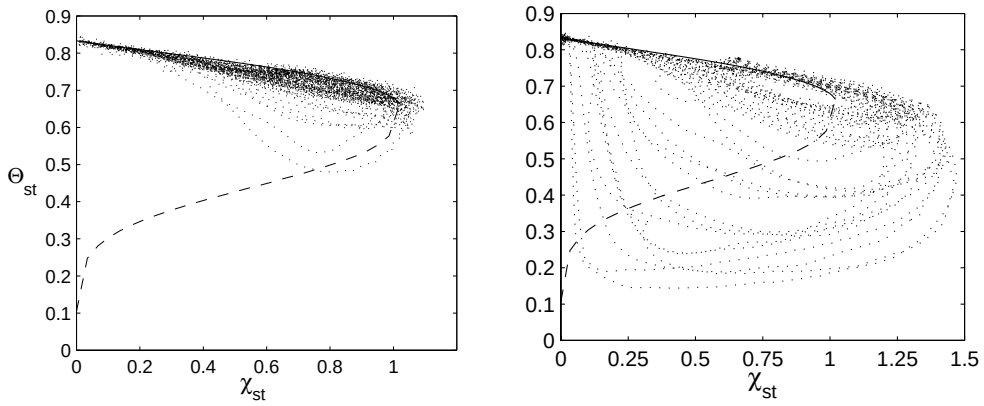

FIGURE 4. Particle paths in the $\Theta_{\rm st} - \chi_{\rm st}$ plane. (a) $0.95 < \chi_{\rm max} < 1.1$. (b) $1.2 < \chi_{\rm max} < 1.5$.

early in the simulation, the flame burns vigorously with little extinction and SFL predicts the conditional average well (Fig. 3b).

As more and more flame elements experience scalar dissipation rate values that are higher than $\chi_{\rm q}$ (see Fig. 1), their temperature starts to decrease and the conditionally averaged temperature increasingly deviates from the SLFM prediction (Fig. 3c). At a later time, however, the local values of the scalar dissipation rate starts decreasing. Points whose temperature dropped down when their scalar dissipation rate was larger than $\chi_{\rm q}$ are getting transported back into the $\chi < \chi_{\rm q}$ region of the $\Theta_{\rm st} - \chi_{\rm st}$ plane. Figure 3d demonstrates a bimodal situation where steadily burning and nearly extinguished points exist at identical values of $\chi_{\rm st}$. Eventually, the temperature of the "extinguished" points starts increasing, the conditional average $\langle \Theta | Z_{\rm st}, \chi_{\rm st} \rangle$ starts rebounding, and gradual reignition takes place.

4.2. *Extinction and reignition: flame element tracking*

Figure 4 shows the paths of flame elements in the Θ-χ space over a time interval of t=0-0.50. In the figure the burning branch of the steady flamelet solution is continued into the middle, unstable branch (broken line). Only a few of the flame elements shown in Fig. 4a are associated with χ values that exceed $\chi_{\rm q} = 1.02$. Accordingly, the temperatures in this figure stay close to the steady burning branch at all times. Figure 4b refers to flame elements whose scalar dissipation rate gets higher than $\chi_{\rm q}$; therefore, their temperatures drop below the unstable branch and get reignited from there.

Figure 4 demonstrates that, in the present simulations, the $\chi_{\rm q}$ value derived from the flamelet model is a valid measure of the characteristic value of the scalar dissipation rate that leads to extinction. A similar conclusion has been reached recently by Overholt & Pope (1999).

According to the TFL approach for a fixed value of $\chi_{\rm st}$, any flame element that is above the unstable branch will reignite, while flame elements that are below this branch will extinguish. It follows that crossing the broken line contradicts flamelet modeling†. The reignition observed in Fig. 4b is certainly not the autoignition of isolated flamelets.

† If the flow "moves" the scalar dissipation rate of an element faster than the characteristic times of extinction or reignition, the flamelet can cross the broken line horizontally (Pitsch & Fedotov (2000)).

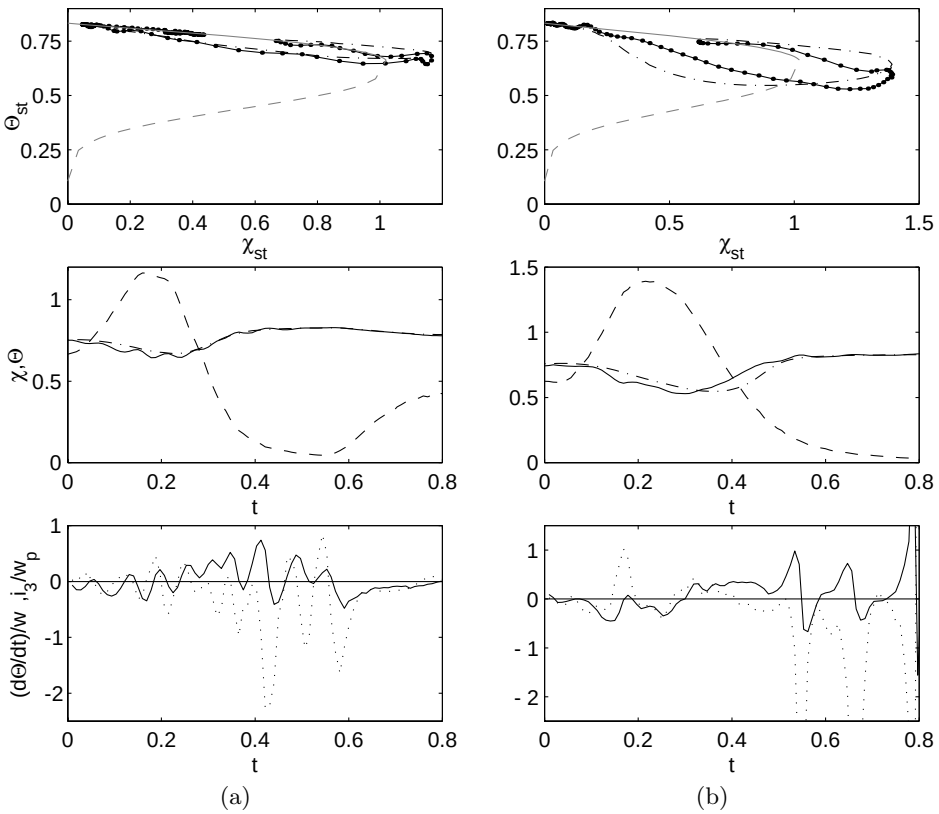

FIGURE 5. Various flame element histories with different patterns of extinction-reignition. Top two figures: ——— : temperature data; —·— : TFL model results; grey ——— and - - - - : burning and unstable branches of the SFL solution; - - - - : scalar dissipation rate. Bottom figure: ——— : $(d\Theta/dt)/w$ from DNS data; ····· : i_3/w term.

Almost all of the flame element temperatures plotted in Fig. 4b are already on the increase when they cross the unsteady branch. Since all the paths shown in Fig. 4b reignite through the broken line, the figure demonstrates that TFL is not consistent with the reignition of flame elements whose scalar dissipation rate at some point in time was well above χ_q.

It is also interesting to note that different flame elements exhibited quite different behavior. Some flame elements reignited fast; other elements did not reignite at all in the time interval considered. Some of these features are expected to be explained by the inclusion of the interaction term, i_3.

A variety of extinction-reignition behavior is shown in Fig. 5-7. In the figures the full line indicates the DNS result, the dash-dot line the TFL calculations, while the respective grey full and broken lines depict the burning and unstable branches of the steady-flamelet (SFL) solution. The DNS and SFL results are denoted similarly in the lower figures, whereas the broken line shows the time evolution of χ_{st}. For the bottom figure, the full line is $(d\Theta/dt)/w$ from the DNS data while the dotted line is the i_3/w term.

In Fig. 5a, χ_{st} exceeds χ_q only slightly and for a short time; in Fig. 5b, χ_{st} exceeds χ_q by a larger margin but still for a relatively short time. TFL predicts the temperature

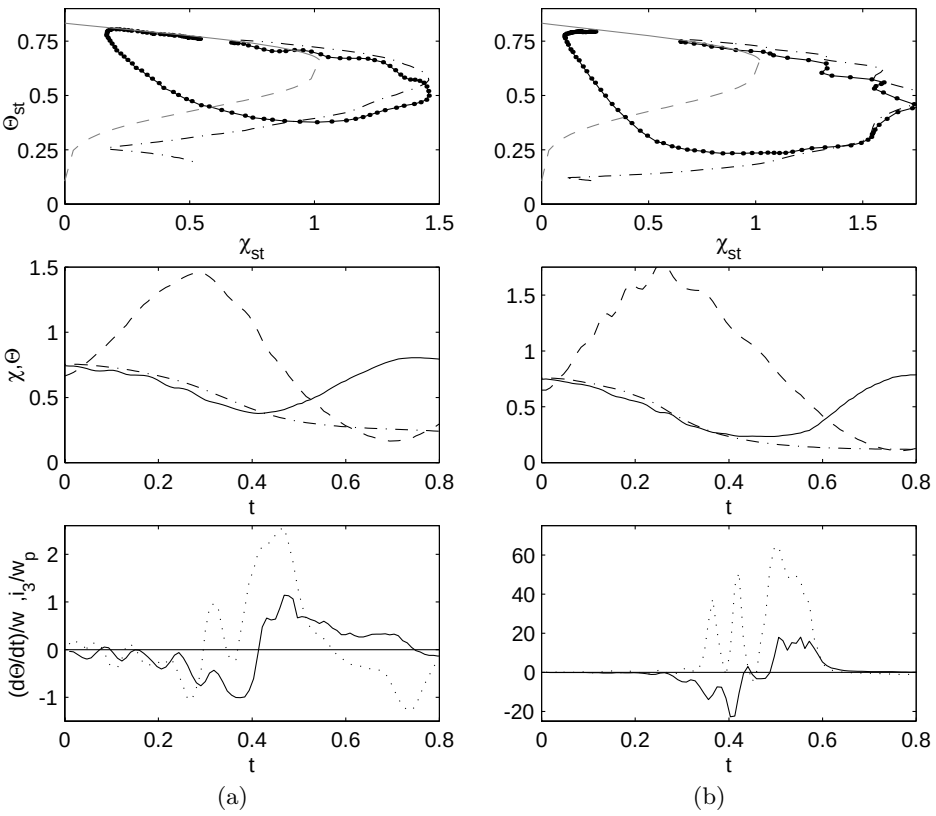

FIGURE 6. (See Fig. 5 for captions.)

correctly in both cases. It is interesting to notice, however, the difference between the data and the flamelet prediction in the uppermost part of Fig. 5b. The flamelet prediction crosses the unsteady branch horizontally (see footnote before), whereas the trace taken from the data shows slightly oblique crossing. This effect is obviously due to neighboring hot flame elements that are not considered in the flamelet approximation. In Fig. 5, the i_3 term is quite small and exerts no major influence on the results.

Figure 6-7 show flame elements undergoing major extinction followed by reignition. TFL predicts the initial extinction process quite well but fails to reignite the flame element except in Fig. 7b. In Figs. 6a,b and 7a, TFL predicts full extinction after the element gets below the unsteady branch. In Fig. 7b the flamelet model reignites due to crossing the broken line horizontally, but the data show very different behavior.

We believe that the reignition process in Figs. 6 and 7 is influenced by hot flame elements in the vicinity of the flame element we are following. Our expectation has been that i_3 would exhibit a positive peak at the time when the temperature of the extinguished element starts to increase. Physically speaking, the expectation is that it is a "bump" in i_3 that helps the flame element to cross the unsteady branch.

Close inspection of the $i_3(t)$ time evolution in Figs. 6 and 7 indeed shows behavior reminiscent of the expected behavior, but the effect seems to be influenced by resolution errors. We will investigate the matter further using better resolution.

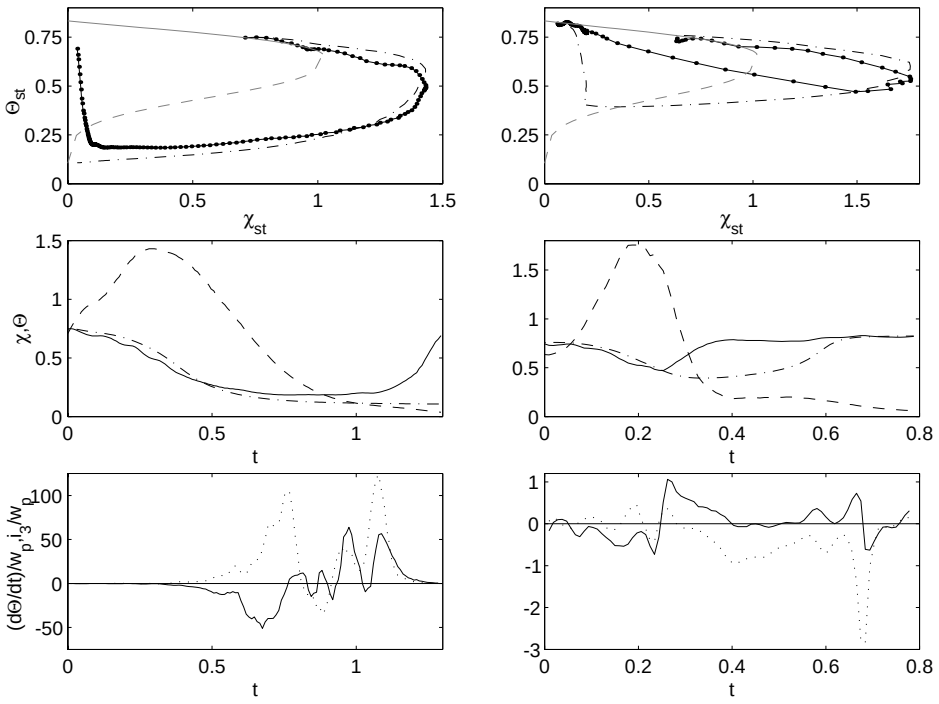

FIGURE 7. (See Fig. 5 for captions.)

5. Conclusions and future work

Direct numerical simulations have been performed to investigate the local extinction-reignition of initially nonpremixed fields of fuel and oxidant. The extinction-reignition process is due to the increase and decrease of the scalar dissipation rate caused by the initial strong straining followed by the dominance of molecular diffusion. To elucidate the applicability of the flamelet modeling, the entire time history of different fluid elements (points fixed on the $Z_{\rm st}$ surface) have been tracked. An extended flamelet model has been introduced that contains a term (i_3 in Eq. (3.10)) that accounts for lateral heat diffusion along the $Z_{\rm st}$ surface.

The results shows that the extinction criterion derived from flamelet modeling ($\chi_{\rm st} > \chi_{\rm q}$) works well. The data demonstrate, furthermore, that time dependent flamelet modeling correctly predicts the behavior of flame elements with little or no extinction. Even the extinction phase of the history of a flame element is captured by the model, approximately. Standard flamelet modeling was found to break down during reignition.

In flamelet modeling the flame elements extinguish and reignite as separated counterflows. We believe that this is the reason behind the failure of the model to describe reignition correctly. Our expectation is, therefore, that the $i_3(t)$ term in Eq. (3.10) has a decisive role in the reignition process. Due to our limited resolution, we could not confirm this behavior. Presently we are working on a better resolved simulation that will clarify this issue. We are also planning to use the new simulations to study the influence of (a) premixed pockets created by mixing in extinguished regions and (b) the interaction between extinguished and burning flame elements due to curvature.

Acknowledgments

Paiboon Sripakagorn's stay at CTR was supported by ASCI and CTR. George Kosály's sabbatical stay at Stanford is partially supported by CTR.

REFERENCES

Elghobashi, S. & Truesdell, G. C. 1993 Direct simulation of particle dispersion in a decaying isotropic turbulence. *J. Fluid Mech.* **242**, 655-700.

Eswaran, V. & Pope, S. B. 1988 Direct numerical simulations of the turbulent mixing of a passive scalar. *Phys. Fluids.* **31**, 506.

Gibson, C. H. 1968 Fine Structure of Scalar Fields Mixed by Turbulence. I. Zero-Gradient Points and Minimal Gradient Surfaces. *Phys. Fluids.* **11**, 2305.

International Workshop on Measurement and Computation of Turbulent Nonpremixed Flames 2000. *http://www.ca.sandia.gov/tdf/Workshop.html.*

Lee, Y. Y. & Pope, S. B. 1995 Nonpremixed Turbulent Reacting flow near Extinction. *Comb. Flame.* **101**, 501-528.

Mell, W. E., Nilsen, V., Kosály, G. & Riley, J. J. 1994 Investigation of closure models for nonpremixed turbulent reacting flows. *Phys. Fluids A.* **6**, 1331.

Nilsen, V. 1998 *PhD thesis,* Mechanical Engineering Department, University of Washington, Seattle, WA.

Overholt, M. R. & Pope, S. B. 1999 Direct numerica simulation of a statistically-stationary, turbulent reacting flow. *Combust. Theo. Modeling.* **3**(2), 371-408.

Peters, N. 1983 Local Quenching Due to Flame Stretch and Non-Premixed Turbulent Combustion. *Comb. Sci. Tech.* **30**, 1-17.

Peters, N. 1984 Laminar diffusion flamelet models in non-premixed turbulent combustion. *Prog. Energy Combust. Sci.* **10**, 319-339.

Peters, N. 2000 Turbulent combustion. *New York, Cambridge University Press.*

Pitsch, H. & Fedotov, S. 2000 Investigation of Scalar Dissipation Rate Fluctuations in Non-premixed Turbulent Combustion Using a Stochastic Approach. *Comb. Theo. Modeling.* Submitted for publication.

Sato, Y. & Yamamoto, K. 1987 Lagrangian measurement of fluid-particle motion in an isotropic turbulent field *J. Fluid Mech.* **175**, 183-199.

Shlien, D. J. & Corrsin, S. 1974 A measurement of Lagrangian velocity auto-correlation in approximately isotropic turbulence *J. Fluid Mech.* **62**, 255-271.

Squires, K. D. & Eaton, J. K. 1991 Lagrangian and Eulerian statistics obtained from direct numerical simulations of homogeneous turbulence. *Phys. Fluids A.* **3**, 130-143.

Yeung, P. K. & Pope, S. B. 1988 An Algorithm for Tracking Fluid Particles in Numerical Simulations of Homogeneous Turbulence. *J. Compt. Phys.* **79**, 373-416.

Yeung, P. K. & Pope, S. B. 1989 Lagrangian statistics from direct numerical simulation of isotropic turbulence. *J. Fluid Mech.* **207**, 531.

Xu, J.& Pope, S. B. 1999 Assessment of numerical accuracy of PDF/Monte Carlo methods for turbulent reacting flows. *J. Comp. Phys.* **152**(1), 192-230.